Mitigation of SOA-Induced Nonlinearities With Recurrent Neural Networks in 75 Gbit/s/λ PAM-4 IM/DD WDM-PON Transmission Systems

Ahmed Galib Reza, Marcos Troncoso-Costas, *Graduate Student Member, IEEE*, Colm Browning, *Senior Member, IEEE*, Sean O'Duill, and Liam P. Barry, *Senior Member, IEEE*

***Abstract*—We experimentally demonstrate 4 × 75 Gbit/s optically amplified 4-level pulse amplitude modulation (PAM-4) transmission based on an external Mach-Zehnder modulator (MZM) and electro-absorption modulator (EAM) for monolithically integrable intensity modulation and direct detection wavelength division multiplexed passive optical networks (WDM-PONs). The effects of semiconductor optical amplifier (SOA)-induced nonlinear distortions during single- and multi-wavelength amplification in the optical distribution networks are investigated for various channel spacings through experiments and simulations. A machine learning-based nonlinear equalizer termed as a recurrent neural network (RNN) is proposed to compensate for the nonlinear impairments. Finally, by employing a T-spaced RNN in conjunction with a traditional feed-forward equalizer (FFE), we achieve link budgets in excess of 31 dB and 28 dB on every WDM channel at the hard-decision forward error correction (HD-FEC) limit of 3.8×10^{-3} for MZM and EAM-based WDM-PONs, respectively, after 4 × 75 Gbit/s PAM-4 transmissions at 1550 nm with a 100 GHz channel spacing over 25 km feeder and 1 km distribution single-mode fiber links.**

***Index Terms*—4-level pulse amplitude modulation (PAM-4), recurrent neural network (RNN), semiconductor optical amplifier (SOA), wavelength division multiplexing passive optical network (WDM-PON).**

I. Introduction

PASSIVE optical networks (PONs) are the key enabling technologies to meet the latest unprecedented bandwidth demand due to an exponential growth of Internet data traffic driven by the evolution of bandwidth-hungry applications and multimedia services such as the Internet of Things (IoT), Video on Demand (VoD), Voice over Internet Protocol (VoIP), ultra-high-definition video streaming, mobile fronthaul/backhaul networks for 5G+/6G, etc. Recently, the standardization of 25G/50G Ethernet PON (EPON) has been approved by the IEEE 802.3ca task force, which offers 25 Gbit/s transmissions on a single wavelength, and 50 Gbit/s transmissions by combining two wavelengths with a capacity of 25 Gbit/s/λ [1]. The higher-speed PONs of ITU-T G.9804.3 describes a 50 Gbit/s/λ capacity PON with power budgets and optical reach requirements comparable to the previous generation of PONs to ensure coexistence with the legacy PON [2]. For further capacity updates, the development of technology beyond 50G or 100G PONs is still at the research level [3], [4], [5], [6], [7].

The coherent PON can satisfy such capacity requirements [4]; however, the application of the coherent technology is more suitable in the metro and core networks due to its high deployment cost, complexity, and power consumption of digital signal processing (DSP) techniques. The PON market is extremely cost-sensitive, as it provides the last-mile connectivity between an Internet service provider (ISP) and the end-user, and the total costs are directly compensated by the subscribers. In this regard, intensity modulation and direct detection (IM/DD) is the most suitable choice for PONs in the near to medium term due to its simple architecture, compactness, and low deployment cost, compared with the coherent technology.

For a high-speed IM/DD PON, 4 or 8-level pulse amplitude modulation (PAM-4/PAM-8) can be the ultimate choice due to its higher spectral efficiency and simple architecture. To boost the link budget, an optical amplifier such as a semiconductor optical amplifier (SOA) can be a good choice due to its compactness, low cost, ease of integration, and high gain over a wide range of the spectrum [5], [6], [7]. However, the performance of SOA-amplified high-speed PONs is still restricted by the low-modulation bandwidth and nonlinear response of the modulators [8], fiber channel transmission impairments such as attenuation, chromatic dispersion, and self-phase modulation (SPM), and SOA-induced amplified spontaneous emission (ASE) noise at low input power and nonlinear distortions at high input power due to gain saturation and data patterning [9]. In addition, a wavelength-division multiplexed PON (WDM-PON) that employs SOAs can be affected by interchannel crosstalk due to cross-phase modulation (XPM) and four-wave mixing (FWM) [10].

Manuscript received 15 November 2022; revised 16 April 2023; accepted 18 May 2023. Date of publication 22 May 2023; date of current version 27 June 2023. This work was supported in part by Science Foundation Ireland through Research under Grants 18/SIRG/5579, 18/EPSRC/3591, and 12/RC/2276_P2 and in part by the Enterprise Ireland Through Research under Grant DT 2019 0014A. *(Corresponding author: Ahmed Galib Reza.)*

Ahmed Galib Reza, Colm Browning, Sean O'Duill, and Liam P. Barry are with the School of Electronic Engineering, Dublin City University, Dublin 9, Ireland (e-mail: ahmed.galibreza@dcu.ie; colm.browning@dcu.ie; sean.oduill@dcu.ie; liam.barry@dcu.ie).

Marcos Troncoso-Costas is with the School of Electronic Engineering, Dublin City University, Dublin 9, Ireland, and also with the AtlanTTic Research Center, University of Vigo, EI Telecommunication, 36310 Vigo, Spain (e-mail: troncosocostas2@mail.dcu.ie).

Color versions of one or more figures in this article are available at https://doi.org/10.1109/JLT.2023.3278981.

Digital Object Identifier 10.1109/JLT.2023.3278981

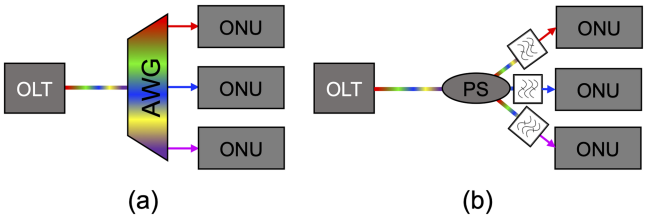

Fig. 1. Basic WDM-PON architectures. (a) AWG-based; (b) PS-based.

The performance of an SOA is governed by the carrier lifetime. During high-speed data transmissions, the symbol period can be considerably shorter than the carrier lifetime of the SOA, which causes an insufficient recovery time. To mitigate such effects, optical filtering [11] and gain clamping [12] have been used over the last few years. Recently, DSP techniques such as digital backpropagation [13], decision feedback equalizer (DFE) [14], Volterra nonlinear equalizer (VNLE) [6], and machine learning (ML) algorithms, e.g., artificial neural networks (ANNs) [15], [16], convolutional neural networks (CNNs) [17], and recurrent neural networks (RNNs) [18] have been proven to be effective in mitigating nonlinear signal distortions.

This article is an extension of our previous works on multi-wavelength amplifications [19] in the remote node (RN) of an SOA-based WDM-PON system, in which using a 1550 nm Mach-Zehnder modulator (MZM), we reported 4 × 75 Gbit/s PAM-4 transmissions over a 25 km feeder fiber (FF) in a 100 GHz spaced WDM channels and verified the significance of RNNs in mitigating nonlinear signal distortions. However, it is important to analyze the performance of electro-absorption modulators (EAMs) in such a WDM-PON system, as it is the most suitable candidate for photonic integration considering the primary materials for fabrication. In this article, we experimentally demonstrate the effectiveness of RNNs in mitigating SOA-induced nonlinearities for MZM- and EAM-based WDM-PON systems and compare their performance in terms of the power budget. In addition, we investigate optimum wavelength spacings for a given data rate, as it is critically required to make efficient use of the scarce wavelength resources.

II. WDM-PON Architectures

Several WDM-PON architectures as well as their operating principle can be found in the literature [20]. In general, depending on the wavelength demultiplexing techniques, there can be two basic WDM-PON architectures. One is to utilize an arrayed waveguide grating (AWG) in the optical distribution networks (ODNs), which offers low insertion loss (typically 5 dB) and is independent of the number of wavelengths, as shown in Fig. 1(a). However, the deployment cost of an AWG-based demultiplexing scheme radically increases as the number of output ports grows. The other option is power splitting by employing a passive splitter (PS) in the ODN, as illustrated in Fig. 1(b), followed by placing an optical filter at the ODN/optical network units (ONUs) to select one of the wavelengths. Nonetheless, the number of ONUs the network can support is highly dependent on the splitting losses in the ODN. In a WDM-PON system, the ONU serves as an access point for the customers and is usually deployed in a cabinet at the customers' premises or on the street. Therefore, it is essential to expand the number of ONUs in the PON. Considering the current deployment difficulty and budget requirements for the AWG-based WDM-PON, the splitter-based WDM-PON architecture is preferable, as it can co-exist with the legacy time-division multiplexed-PON (TDM-PON).

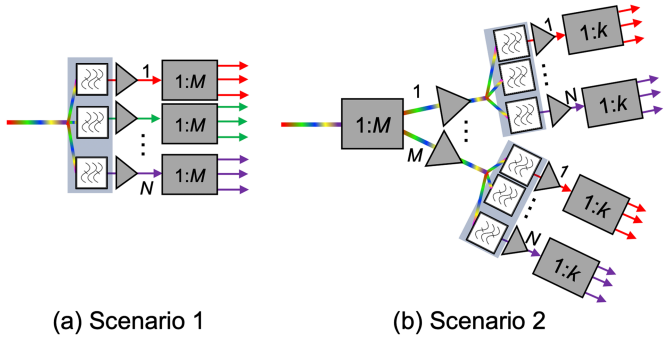

Fig. 2. Concept of optical amplifications in the ODN of a WDM-PON. (a) Single-channel amplifications; (b) *N*-channel amplifications.

A. Optically Amplified WDM-PONs

The next-generation IM-DD WDM-PON must support a high data rate and large power budget requirements of 29–32 dB. Providing such a power budget is an obvious problem as the data rate increases. Therefore, the incorporation of optical amplifiers in the network might be essential. The optical amplifiers can also enhance the number of splitting stages in the network to boost the number of ONUs. For example, in Fig. 2, two optically amplified WDM-PON scenarios are shown.

In scenario 1 (Fig. 2(a)), it is shown that after demultiplexing of N WDM channels, if the signal power of every WDM channel can be boosted by an optical amplifier, it can support up to M-connected ONUs in a point-to-multipoint fashion. Therefore, a single-stage splitting in the network can support up to $M \times N$ ONUs.

Another PON scenario is presented in scenario 2 (Fig. 2(b)) where the entire N-channel WDM spectrum is amplified using a high-gain optical amplifier and broadcasted to all the connected ONUs in the network by a $1 \times M$ PS. This architecture will enable a second-stage splitting in the network, and each branch with N WDM channels can serve k ONUs. Consequently, the second-stage splitting can provision $k \times N \times M$ number of ONUs. Compared with scenario 1, scenario 2 can potentially increase the number of users in the network at the cost of significant nonlinearity in the system due to FWM, SPM, and XPM in the employed amplifiers.

It is worth noting that the utilization of optical amplifiers and PSs in the PON will enable both architectures to share one wavelength between several ONUs in the network in a TDM fashion, which can also reduce both deployment cost and power consumption of the transceivers. In other words, the TDM technique can be implemented in the PON along with the WDM, which is also called TWDM-PON.

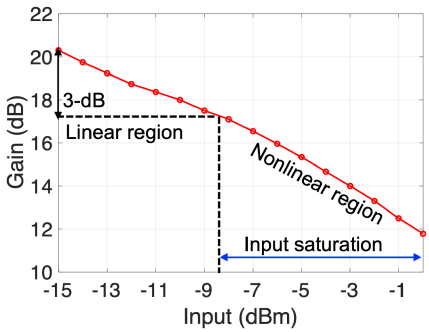

Fig. 3. SOA gain as a function of the input power into the SOA.

TABLE I
SIMULATION PARAMETERS USED FOR THE SOA MODELLING

Symbol	Definition	Value (units)
h_0	Total small signal gain	6 (a.u.)
$\alpha_L L$	Total waveguide scattering losses	3 (a.u.)
α_H	Gain-phase coupling parameter	3 (a.u.)
P_{sat}	Saturation power	20 (mW)
τ_c	Effective carrier lifetime	200 (ps)
ε_{SHB}	Inverse of the SHB saturation power	1 (W^{-1})
ε_{CH}	Inverse of the CH saturation power	2 (W^{-1})
α_{CH}	CH-phase coupling parameter	-1 (a.u.)
n_{sp}	Spontaneous emission factor	3 (a.u.)

B. Semiconductor Optical Amplifiers

For optical amplification, the use of an SOA in the RN can be essential because of its integrability, low cost, low power consumption, and high gain. However, one critical problem due to SOA-based amplifications in a WDM-PON system is nonlinear signal distortion caused by the patterning effects in the gain saturation region of the SOA. The nonlinear response of an SOA can be expressed as [21]

$$E_{out} = E_{in} \exp\left(\frac{h}{2}(1 + j\alpha_H)\right) \tag{1}$$

where E_{in} and E_{out} respectively represent the input and output electrical fields of the SOA, h is the gain exponent, α_H is the linewidth enhancement factor, and j is an imaginary unit.

The time-dependent gain g of the SOA can be expressed as [21]

$$\frac{dh}{dt} = \frac{h_0 - h}{\tau_c} - \frac{h\left(\exp\left(h - \alpha_L L\right) - 1\right)}{h - \alpha_L L}\frac{|E_{in}|^2}{P_{sat}} \tag{2}$$

where τ_c is the carrier lifetime, h_0 is the unsaturated amplifier gain, $\alpha_L L$ is the product of the loss coefficient and the length of the cavity, and P_{sat} is the saturation output power of the SOA.

Fig. 3 illustrates the gain of the SOA (Kamelian OPB-10-15-N-C-FA) used in our experiments as a function of the input optical signal power. We set the bias current of the SOA at 150 mA and operate it at 25 °C. It can be seen that the SOA gain decreases as the input signal power increases and the 3 dB compression point ($P_{3\text{dB}}$) is found at an input power of around -8.2 dBm. In general, if the input signal power into the SOA goes below/above the $P_{3\text{dB}}$ of -8.2 dBm, the SOA-induced ASE noise/strong pattern-dependent effects due to gain saturation begins to dominate the system performance, respectively [22]. In some cases, multi-level signals, such as PAM-4, may impose a higher linearity requirement in the system and it may be suitable to reduce the SOA output power by restricting the SOA to operate at a 1 dB compression point [23]. This work finds the optimum input power into the SOA for PAM-4 signals in a WDM-PON transmission scenario, which will take into account both ASE-induced distortion in addition to the nonlinearity effects relevant for both single and multi-wavelength amplification.

III. SIMULATION FOR CROSSTALK INVESTIGATION

In this section, we optimize the WDM channel spacing for SOA-amplified 4 × 37.5 GBaud WDM-PONs by undertaking a simulation in MATLAB to model the overall behavior of the experimental system. The simulation considers the sampling rate, the bandwidth limitations of various optical/electrical components, the nonlinear transfer function of an MZM, the electrical noise in the driving signal, the amplitude and phase noise of the laser output, and the ASE noise of the EDFA. For simplicity of implementation, the bandwidth limitations were modeled as raised-cosine filters with a roll-off factor of 0.2. The fiber propagation was modeled by numerically solving the nonlinear Schrödinger equation accounting for second and third-order dispersion, SPM, XPM, and FWM. Direct detection was modeled in the simulation considering the photocurrent, thermal noise, shot noise, and dark current. The effective resolution of the analog-to-digital converter (ADC) is 8-bit.

In the simulation, the SOA dynamics are approximated using the Lumped model [21]. To keep a moderate computational complexity, the effects of carrier heating (CH) and spectral hole burning (SHB) are included in the simulation using the adiabatic approximation. Table I presents the parameters used in the simulation to model the SOA across various transmission scenarios. We request the reader to refer to ref. [21] for the inclusion of CH, SHB, and ASE into the dynamic equations.

Four independent pseudorandom multi-level sequences 2^{20} symbols long are used to generate the 37.5 GBaud PAM-4 signals. The channel spacings of 50 GHz, 100 GHz, and 200 GHz are studied to investigate the two scenarios of optically amplified WDM-PONs, as discussed in Section II. In the simulation, the four channels centered at 193.1 THz are utilized to transmit over 25 km of FF with an attenuation factor of 0.2 dB/km, dispersion coefficient of 5 ps/(nm∗km), dispersion slope of 0.08 ps/(nm^2∗km), and nonlinear coefficient $\gamma = 1.3$ W/km. The total launch power into the fiber is 13 dBm, and the per-channel launch power is set to 7 dBm. Two scenarios are simulated and analyzed after 25 km fiber transmissions: (1) demultiplexing of channel 2 followed by optical amplifications and transmissions over a 1 km DF; (2) Amplifications of the 4-channel WDM spectrum by a single optical amplifier followed by demultiplexing of channel 2 before transmitting over a 1 km DF. An optical filter with a 3 dB bandwidth of 50 GHz and an extinction ratio of 37 dB is

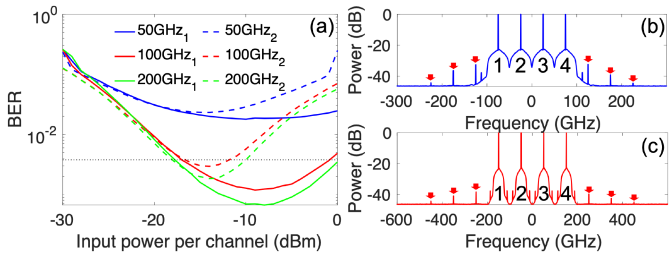

Fig. 4. (a) BER at an ROP of −6 dBm versus input signal power per channel into the SOA for various channel spacings. The BERs for scenarios 1 and 2 are denoted by the solid and dashed lines, respectively. The optical spectra of four-wavelength WDM-PONs centered at 193.1 THz for scenario 2 in the case of (b) 50 GHz, and (c) 100 GHz channel spacings.

used to filter a WDM channel. The filter has a sharp rejection property from the passband to the stopband (replicating the common transmission profiles of commercial filters), and the pass and the stopbands were assumed ripple-free. To ensure accurate numerical integration of the fiber propagation and SOA dynamics, as well as to have enough simulation bandwidth to accommodate all the FWM terms, the time steps of the simulation are set to 5/3 ps, 5/6 ps, and 5/12 ps for the channel spacings of 50 GHz, 100 GHz, and 200 GHz, respectively. At the receiver, the received signals are resampled to one sample per symbol, and a conventional T-spaced 21-tap FFE is applied for symbol equalizations [24]. Initially, the FFE enters a training phase and adapts the tap coefficients using a training sequence. Finally, the bit error ratio (BER) is calculated by counting errors.

Fig. 4(a) shows the BERs obtained at a received optical power (ROP) of −6 dBm at the square-law photodetector (PD) for scenarios 1 and 2 as a function of input power per channel into the SOA. The BER results demonstrate that the effects of SOA-induced nonlinearities are lower in scenario 1 compared with scenario 2, leading to much better performances for any channel spacings. The performance for 50 GHz spacing is poorer even at low SOA input powers because of the high launch power of 13 dBm into the fiber and increased inter-channel nonlinearity in the fiber, particularly FWM which increases sharply with a narrower channel spacing and an increased launch power. As no saturation was included in the receiver model, resulting in performance degradation at low powers and stable performance after thermal noise from PD becomes negligible. With 50 GHz spacing, the hard-decision forward error correction (HD-FEC) limit BER performances cannot be reached in both scenarios. Meanwhile, with 100 GHz spacing, scenario 2 only works for an input power variation of 5 dB (−11.8 dBm to −16.8 dBm). We notice a marginal improvement in the performance when the channel spacings are increased from 100 GHz to 200 GHz. The optical spectra presented in Figs. 4(b) and (c) for scenario 2 in the case of 50 GHz and 100 GHz channel spacings, respectively, can verify our BER results as the undesired FWM components appear stronger and closer to the desired passband when the channel spacings become narrower.

The numerical results presented in Fig. 4(a) indicate that the impact of SOA-induced nonlinearity is greater in scenario 2, and 100 GHz channel spacing can be the optimal choice considering the trade-off between the performance and spectral efficiency. We note that the performance of such a WDM system is typically limited by the fiber and SOA nonlinearities; therefore, further improvements in the BER performances can be achieved by applying a nonlinear equalizer in the receiver DSP.

IV. Experimental Setup

In Fig. 5, we present the experimental setup for a four-wavelength WDM-PON system. Based on two different optical modulators (MZM and EAM), two distinct 75 Gbit/s/λ WDM-PON systems with a total capacity of 300 Gbit/s are experimentally demonstrated and analyzed in this work. At the transmitter side, four narrow linewidths (less than 100 kHz) tunable external cavity lasers (ECLs) are utilized in the experiment. For the WDM transmission experiments, the output power of the four ECLs is set to 10 dBm, and each ECL operates in the frequency range of 192.95 THz to 193.35 THz with 100 GHz channel spacing, as optimized in the simulation.

At the transmitter, four ECLs are evenly partitioned into two groups. The CW (continuous wave) lights from the two ECLs in each group are combined using a 2 × 1 PS. In the case of MZM, a polarization controller (PC) is used after the PS to set the state-of-polarization of the light. For EAM, a PC is not required, as it has less polarization dependence. Next, the outputs of the two PCs/PSs from each group are combined by another 2 × 1 PS to generate a 100 GHz spaced four-wavelength WDM signal with an optical power of 10 dBm.

Subsequently, for the MZM-based system, the combined ECL outputs are modulated by a single-ended 20 GHz MZM (3 dB bandwidth), which is biased at the quadrature point and driven by 37.5 GBaud PAM-4 signals. However, for the EAM-based system, it is required to apply a reverse bias to the EAM to achieve a reasonable extinction ratio, which is provided by adding a separate DC bias tee between the driver and EAM. In Figs. 5(a) and (b), we present the nonlinear transfer curve of the MZM and EAM at 193.3 THz, respectively. As expected, we can see that the MZM transfer function is cosine shaped. In Fig. 5(b), we notice that as the reverse bias increases, the EAM attenuation also increases. In the experiment, the EAM is reverse biased at 1.45 V. We note that the EAM produces about 10 dB insertion loss when no biasing is applied, which can be improved by photonic integration.

To compensate for the modulation insertion loss, a low-noise erbium-doped fiber amplifier (EDFA) is utilized on the transmitter side to set the signal power to 13 dBm before launching into a 25 km feeder single-mode fiber (SMF), which corresponds to 7 dBm launch power per WDM channel. Although the EDFA can deliver a total output power of 22 dBm, the launch power is reduced using an optical attenuator to minimize back-reflection caused by the stimulated Brillouin scattering (SBS) and system penalties due to FWM, and XPM.

To generate 37.5 GBaud PAM-4 signals, in the transmitter-side offline DSP, the pseudo-random bit sequence (PRBS) is generated and mapped into Gray-coded PAM-4 symbols in MATLAB. After digital upsampling by a factor of 2.25, a root-raised cosine (RRC) pulse shaping filter with a roll-off

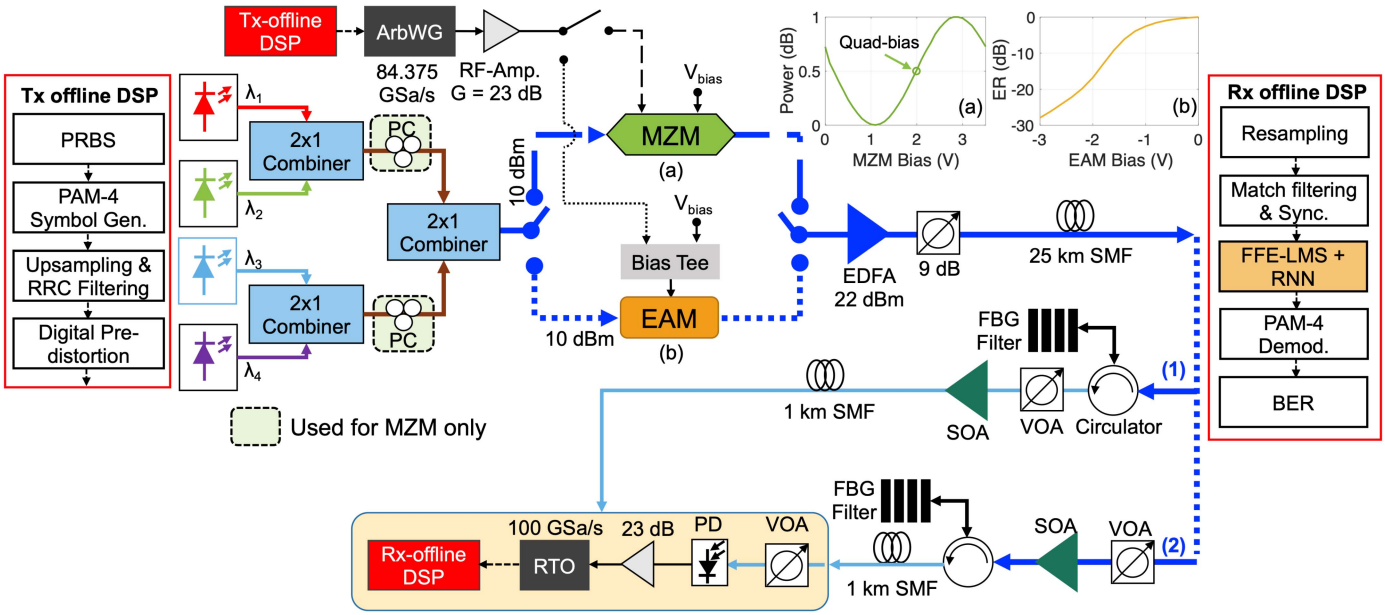

Fig. 5. 4 × 75 Gbit/s optically amplified WDM-PON transmissions using external modulation over a 25 km FF and 1 km DF links.

factor of 0.1 is applied to reduce the signal bandwidth. To achieve equally spaced PAM-4 symbol levels after modulation, the same digital pre-distortion technique is applied to both MZM and EAM-based systems that respect the theoretical nonlinear transfer function of the MZM and EAM. Next, the PAM-4 signals are loaded to an 84.375 GSa/s arbitrary waveform generator (ArbWG) with 32 GHz analog bandwidth. The peak-to-peak voltages (Vpp) of the ArbWG are set at 150 mV and 75 mV for the case of MZM- and EAM-based WDM-PON systems, respectively. Finally, the ArbWG output is amplified by a 23 dB gain RF amplifier, which is used to drive the optical modulators.

After transmission over 25 km of an FF, we investigate two scenarios in the network for the SOA-based optically amplified WDM-PONs, as discussed in Section II. In the experiment, although all the data channels modulated onto optical carriers with different wavelengths carry the same information, the transmission over a 25 km FF ensures the decorrelation of the data patterns on adjacent channels. Based on the position of the SOA in the RN, two scenarios are investigated in the experiments:

1) *SOA amplification of a single wavelength* - First, the wavelength demultiplexing of one of the WDM channels is realized in the RN followed by a variable optical attenuator (VOA) to adjust the input signal power into the SOA. Next, the demultiplexed wavelength is amplified using an SOA to boost the power budget and compensate for the splitter loss. Finally, the amplified wavelength is transmitted over a 1 km distribution fiber (DF) link. This TWDM-PON architecture enables the network to share one wavelength with a group of multiple ONUs in a time-sharing fashion.
2) *SOA amplification of the four wavelengths*- We emulate a case where by using a VOA we presumably split the entire WDM spectrum with a 1:*M* PS followed by SOA amplifications of the full 4-wavelength WDM spectrum, wavelength demultiplexing, and transmissions over a 1 km DF. As discussed in Section II, this architecture stimulates the network to utilize a second-stage splitting so that one wavelength can be shared with multiple ONUs across multiple groups in geographically dispersed locations. This TWDM configuration can potentially increase the number of supported users. However, as obtained in the simulations, it brings a significant nonlinearity in the system due to strong nonlinear interactions between the WDM channels and SOA-induced nonlinearities.

In the experiment, the demultiplexing is realized using a three-port optical circulator followed by a fixed wavelength reflective FBG filter with a central frequency of 193.25 THz. The key motivations for using an FBG filter for demultiplexing are low insertion loss, small size, and design simplicity. By tuning the wavelengths of the ECLs (tune in relation to the fixed wavelength FBG), the performances of the two WDM channels namely, the middle and edge channels are decoded and measured in the experiments.

At the receiver, the received optical signal is detected by a 70 GHz photodetector (PD) with a responsivity of 0.6 A/W. To adjust the ROP, a VOA is placed before the PD. Next, the detected signal is amplified using a 23 dB gain RF amplifier, which is captured using a 33 GHz real-time oscilloscope (RTO) running at 100 GSa/s. Finally, the received digital PAM-4 samples are sent to the receiver side offline DSP (Rx-DSP) block for signal recovery that includes resampling of the signals, matched-filtering, symbol synchronization, and digital equalization to mitigate the linear and nonlinear distortions in the signals. For digital equalization, after calculating the filter tap weights using a training sequence, we apply a T-spaced 31-tap FFE followed by a T-spaced RNN consisting of 11 input nodes, a single hidden layer with 25 hidden nodes, and 1 output node. The activation function for the hidden layer is a hyperbolic tangent, while a simple linear function is used in the output layer. It is worth mentioning that

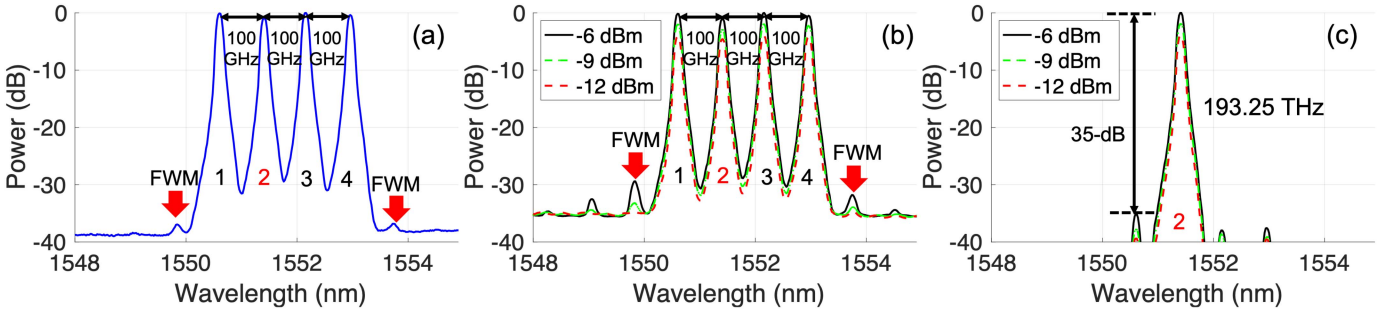

Fig. 6. Measured optical spectra after fiber propagation over a 25 km feeder SMF link; (a) before SOA amplifications, (b) after SOA amplifications, and (c) after SOA amplifications and wavelength demultiplexing.

the overfitting phenomenon of ML does not raise any particular concern in this case, as the number of neurons in the hidden layer is limited. Besides, different training and test datasets are used in the experiment with a limited number of epochs to train the equalizer and performance analysis. Finally, after PAM-4 symbol decoding, the BER performance is measured through error counting.

V. Experimental Results

A. 4 × 75 Gbit/s MZM-based WDM-PON Systems

This subsection presents the experimental results of 4 × 75 Gbit/s WDM-PON design using an MZM. In Fig. 6(a), after fiber transmissions over a 25 km FF link, the measured optical spectrum is shown before SOA amplifications in the RN. The estimated attenuation coefficient of the fiber is about 0.2 dB/km. We can see that there are four WDM channels in the spectrum with a channel spacing of 100 GHz, which has been optimized in the simulation. It is also found that 13 dBm launch power is evenly distributed to all four WDM channels, and the central frequencies of the four channels are 193.35 THz, 193.25 THz, 193.15 THz, and 193.05 THz. We observe that due to the high launch power into the fiber, new frequency components are generated during transmission as a consequence of the FWM in the nonlinear fiber. Furthermore, the equally-spaced WDM channels can significantly worsen the effects of the FWM, as the beating product terms generated by the FWM can fall exactly at the desired electrical passband.

In Fig. 6(b), the FWM effects for various input signal powers into the SOA are investigated for amplifications of the entire spectrum. A substantial increase in the SOA-induced nonlinearity can be observed when the input signal power (−6 dBm) into the SOA falls in the nonlinear region. When the input signal power is moderate (−9 dBm) and falls in the linear region from an SOA gain profile perspective, the nonlinear distortions due to the FWM can be reduced substantially at the expense of optical power attenuation. At a low input power (−12 dBm), the presence of FWM can be concealed and buried under the dominant ASE noise from the SOA, which dictates the WDM system performance. Fig. 6(c) presents the spectrum of the demultiplexed WDM channel with a central frequency of 193.25 THz. An out-of-band rejection ratio of 35 dB from the FBG filter guarantees low interchannel crosstalk, meaning no significant additional penalty.

In Fig. 7, the BER results for MZM-based WDM-PON transmissions are presented. In the figures, the BER performances of the unequalized and equalized PAM-4 signals with an FFE and FFE+RNN are presented by the pentagon, square, and diamond markers, respectively. In Figs. 7(a) and (b), we show the BERs at an ROP of −5 dBm versus various input powers into the SOA for scenario 1 (DeMux+SOA) and scenario 2 (SOA+DeMux), respectively. In both scenarios, the SOA (Kamelian OPB-10-15-N-C-FA) is biased at a fixed current of 150 mA; as we know that higher injection currents can result in higher ASE noise, and only a small additional gain was observed by further increasing the bias current. We can see that the unequalized PAM-4 signals cannot meet the required BER performance level in both scenarios for any SOA input power, as the performances are severely affected by the bandwidth limitations of the modulators [8], transmission impairments such as chromatic dispersion, SPM, and FWM, and SOA-induced ASE noise and gain saturation. However, as observed in the simulation study, we can see that the SOA causes substantial nonlinear crosstalk in the system, especially in scenario 2 (Fig. 7(b)), and a linear FFE alone is not enough to keep the BER performance below the HD-FEC limit of 3.8×10^{-3} with a reasonable power budget. In association with an FFE, a powerful nonlinear equalizer such as an RNN can effectively mitigate critical nonlinear distortions produced at high input powers into the SOA, as a noteworthy improvement in the performance is observed in both scenarios when applying the FFE+RNN compared with just the FFE. The dominance of ASE noise in the system performance can be observed from −12 dBm SOA input power or below, as the BER performances cannot reach the HD-FEC limit (Fig. 7(a)), even when equalized with an FFE+RNN. These results demonstrate that the ML-based RNN cannot reduce the SOA-induced ASE noise level, which could have been enhanced by the linear FFE during the initial equalization process [25]. In Fig. 7(b), we can see that if the input power into the SOA goes above −9 dBm, it can generate excessive nonlinear inter-channel crosstalk, and the HD-FEC level BER performances cannot be achieved with an FFE. From Figs. 7(a) and (b), we can conclude that the optimum input powers into the SOA for scenarios 1 and 2 are −8 dBm and −9 dBm, respectively.

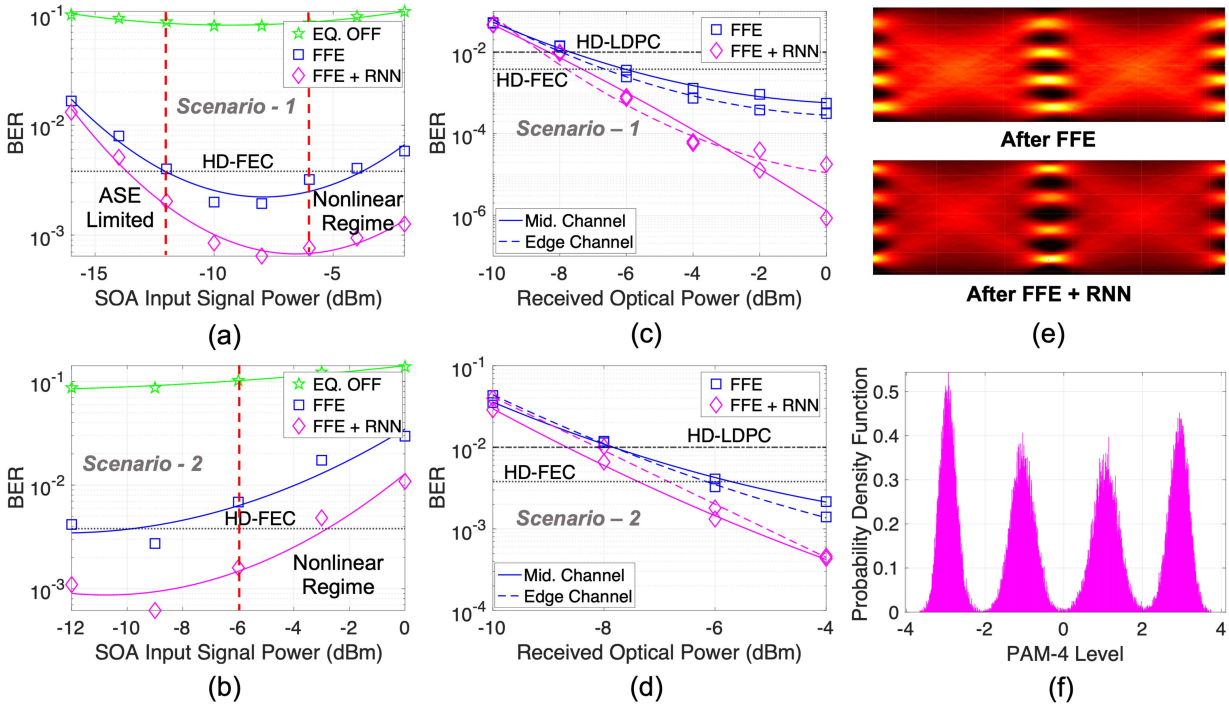

Fig. 7. Experimental results for SOA-amplified PAM-4 modulated 4 × 75 Gbit/s WDM-PON transmission systems using an MZM. BERs as a function of various input powers into the SOA at ROP = −5 dBm when the WDM-DeMux is placed (a) before (scenario 1: single-wavelength amplifications), and (b) after the SOA (scenario 2: four-wavelength amplifications). BERs versus ROPs after T-spaced equalizations with an FFE and an FFE+RNN for (c) scenario 1, and (d) scenario 2. (e) Eye diagrams after FFE and FFE+RNN at an ROP of −4 dBm (f) A histogram of the recovered PAM-4 symbols with an FFE+RNN at an ROP of −4 dBm.

The measured BER results versus ROPs of the WDM channels for scenarios 1 and 2 are shown in Figs. 7(c) and (d), respectively. In the figures, the performances of the middle and edge channels are represented by the solid and dashed lines, respectively. In the context of a 4-wavelength WDM-PON system, the channels denoted by 1 and 4 in the WDM spectra presented in Fig. 6 are the edge channels, while channels 2 and 3 are the middle channels. As optimized in Figs. 7(a) and (b), the input powers into the SOA are set at −8 dBm and −9 dBm for scenarios 1 and 2, respectively. From the BER performance curves in Fig. 7(c), we can see that the FFE+RNN shows the best performance with attainable power budgets of 31.4 dB and 31.9 dB at the HD-FEC level BER for the middle and edge channels, respectively. Considering the hard-decision low-density parity-check (HD-LDPC) decision threshold of 1.0×10^{-2}, chosen by the IEEE 802.3ca [1], the power budgets for the middle and edge channels can be improved by 1 dB and 0.8 dB, respectively, when equalized with an FFE+RNN. The power budgets are calculated by subtracting the sensitivity requirements at the HD-FEC/HD-LDPC level BER performances from the signal launch power into the fiber and adding the SOA gain. In this case, the SOA gain is the logarithm of a power ratio of SOA output power to input power under data modulation. The FFE+RNN can provide gains of about 1.3-dB (mid. ch.) and 1.1-dB (edge ch.) in comparison with the FFE only at the BER of 3.8×10^{-3}. Similarly, in scenario 2 (Fig. 7(d)), the FFE+RNN shows acceptable levels of robustness against nonlinear distortions and achieves optical gains of about 1.7-dB (31.9-dB power budget) and 0.7-dB (31.35-dB power budget) for the middle and edge channels, respectively, at the HD-FEC limit. We note that at the HD-LDPC decision limit, the FFE+RNN can further enhance the power budgets by about 1.2 dB for both middle and edge channels compared with the HD-FEC decision threshold. In addition, the trend shows that the performance gains for the FFE+RNN can improve noticeably at higher ROPs compared with the FFE. In Fig. 7(e), the examples of PAM-4 eye diagrams are shown after FFE and FFE+RNN at an ROP of −4 dBm. The eye diagrams show that the FFE can only correct the linear distortions, and the residual nonlinear distortions can be diminished when applying an RNN, as the FFE+RNN provides a much cleaner and broader eye-opening compared with the FFE. Furthermore, we can observe equally spaced PAM-4 symbol levels in the eye diagrams, indicating that the transmitter-side digital pre-distortion technique can successfully compensate for the nonlinear response of the optical modulators. Fig. 7(f) shows the histogram of the recovered PAM-4 signals for the edge carrier after applying FFE+RNN at an ROP of −4 dBm. In the histogram, the clear and non-overlapping probability density function (PDF) of the PAM-4 symbols indicate the effectiveness of FFE+RNN in mitigating any linear and nonlinear inter-symbol interference (ISI) in the SOA-amplified WDM-PON system.

B. 4 × 75 Gbit/s EAM-based WDM-PON Systems

In Figs. 8(a) and (b), we show the BER results of the EAM-based WDM-PON systems for scenarios 1 and 2, respectively. In the figure, the solid and dashed lines respectively show the BER performances of the middle and edge channels. The square and diamond markers denote the BERs after the FFE and FFE+RNN, respectively. From Fig. 8(a), we can see that the

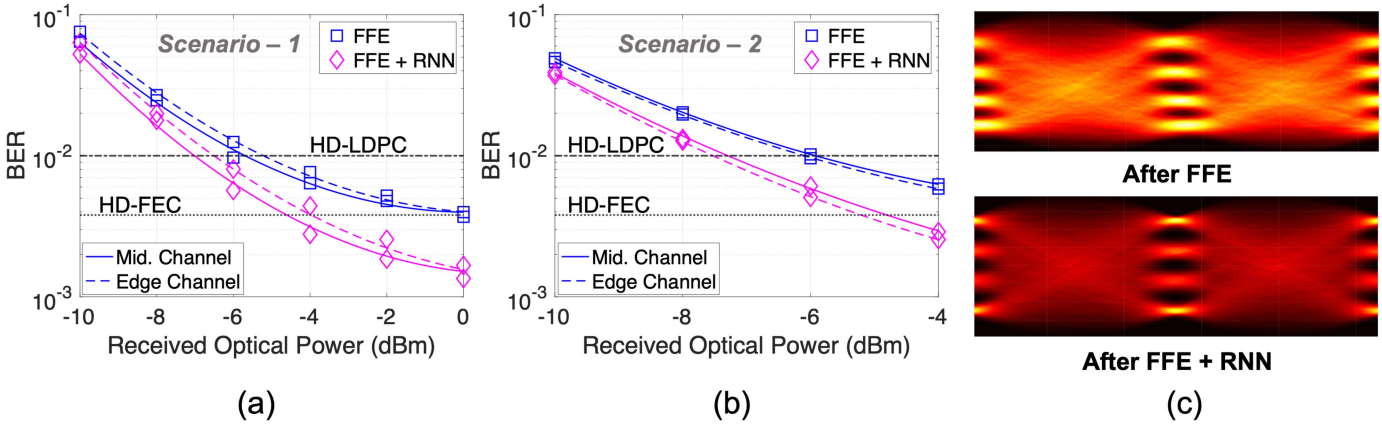

Fig. 8. Experimental results for SOA-amplified PAM-4 modulated 4 × 75 Gbit/s WDM-PON transmissions using an EAM. BERs as a function of ROPs after T-spaced equalizations when the WDM-DeMux is placed (a) before (scenario 1: single-wavelength amplifications), and (b) after the SOA (scenario 2: four-wavelength amplifications). (c) Eye diagrams after FFE and FFE+RNN at ROP = −4 dBm.

FFE can barely touch the HD-FEC level at an ROP of 0 dBm after fiber transmission for both channels. In Fig. 8(b), the FFE fails to reach the required performance levels (both channels), as the nonlinear crosstalk and ROP requirements are higher in this case. However, the FFE+RNN can reach the HD-FEC level performances in both scenarios, indicating that it can mitigate the adverse effects of SOA-induced nonlinearity. In scenario 1, by utilizing an FFE+RNN, we achieve the receiver sensitivity of −4.6 dBm and −4.0 dBm at the HD-FEC BER threshold of 3.8×10^{-3} for the middle and edge channels, respectively. Compared with the HD-FEC BER threshold, the HD-LDPC can provide about 2.5 dB better receiver sensitivity on both channels. For scenario 2, the obtained receiver sensitivities are −4.8 dBm and −5.2 dBm for the middle and edge channels at the HD-FEC performance levels, respectively; indicating a little sensitivity penalty of 0.2 dB (middle channel) and 1.2 dB (edge channel) between scenarios 1 and 2. Depending on the WDM channel position and wavelength, we still observe about 2.3–2.4 dB supplementary gain at the HD-LDPC BER threshold of 1.0×10^{-2} by applying an FFE+RNN.

In summary, from the BER performance curves presented in Figs. 8(a) and (b), we can conclude that after 4 × 75 Gbit/s optically amplified WDM-PON transmissions using an EAM, the FFE+RNN can achieve optical power budgets of about 28.7 dB and 29.3 dB for scenarios 1 and 2, respectively. In comparison with the MZM-based WDM-PON, the EAM-based system experiences a 2–3 dB sensitivity penalty due to an increased nonlinearity in the EAM and extra chirp. Fig. 8(c) shows PAM-4 eye diagrams at an ROP of −4 dBm after applying an FFE and FFE+RNN. The equalized eye diagrams after FFE indicate that the EAM-based system manifests a far more serious eye skewness issue during transmissions compared with the eye presented in Fig. 7(e) for the MZM-based WDM-PON systems. For the EAM, the eye skewness is directly linked to the nonlinear interactions between chromatic dispersion and EAM chirp triggered during absorption. On the other hand, the MZM is almost chirp-free, and dispersion is the only dominating cause of that marginal eye skewness. A deskewed eye diagram in Fig. 8(c) with a cleaner and broader eye-opening indicates that the FFE+RNN can effectively mitigate both linear and nonlinear distortions of the signals induced by the SOA and EAM during multi-wavelength WDM-PON transmissions.

VI. Conclusion

By employing an MZM and an EAM, we experimentally demonstrated two distinct SOA-amplified WDM-PON systems that exploit IM/DD technology for PAM-4 signal transmissions with 75 Gbit/s/λ capacity and 100 GHz channel spacing. Based on the location of the SOA in the RN, we simulate and experimentally investigate the impact of SOA-induced nonlinearities and examine the optimum WDM channel spacings through MATLAB simulation. With FFE+RNN, depending on the transmission situation, we attain power budgets in excess of 31 dB and 28 dB at the HD-FEC limit on every WDM channel after fiber transmissions for MZM and EAM-based WDM-PONs, respectively. A sensitivity penalty of about 2–3 dB is observed for the EAM due to additional nonlinearity, chirp, and dispersion-induced distortions. In conjunction with an FFE in the Rx-DSP, reasonable performances are achieved with a low complexity RNN equalizer, as the dominant linear distortions of the signals are initially mitigated by the FFE before being passed to the RNN equalizer.

In comparison to an avalanche PD (APD)-based ONU receiver design with a tunable filter, the use of an SOA in the RN of the PON can significantly reduce the size, cost, and energy consumption, in addition to the benefits of higher photonic integration at the sub-system or even within the component level. From the integration perspective of the optical modulators used in the system, the integrated EAMs are generally available now, and the development of integrated MZMs using silicon-photonic (SiPh) or thin-film lithium niobate (TFLN) is currently in progress.

In conclusion, the proposed scheme delivers a cost-effective solution to mitigate system nonlinearities and can provide the advantages of photonic integration for an extended reach and/or an extended number of users in future PONs.

REFERENCES

[1] *IEEE P802.3ca 50G-EPON Task Force: Physical Layer Specifications and Management Parameters for 25 Gb/s and 50 Gb/s Passive Optical Networks*, IEEE Std 802.3ca-2020, Institute of Electrical and Electronics Engineers, 2020. [Online]. Available: https://www.ieee802.org/3/ca/

[2] *50-Gigabit-Capable Passive Optical Networks (50G-PON): Physical Media Dependent (PMD) Layer Specification*, Rec. ITU-T G.9804.3, International Telecommunications Union, Geneva, Switzerland, 2021, [Online]. Available: https://www.itu.int/rec/T-REC-G.9804.3-202109-I

[3] J. Li et al., "Demonstration of 200 Gb/s/λ PON in O-band with high-bandwidth TFLN modulator," *J. Lightw. Technol.*, early access, doi: 10.1109/JLT.2023.3256361.

[4] J. Zhang and Z. Jia, "Coherent passive optical networks for 100G/λ-and-beyond fiber access: Recent progress and outlook," *IEEE Netw.*, vol. 36, no. 2, pp. 116–123, Mar./Apr. 2022, doi: 10.1109/MNET.005.2100604.

[5] S. Luo et al., "112-Gb/s/λ downstream transmission for TDM-PON with 31-dB power budget using 25-Gb/s optics and simple DSP in ONU," in *Proc. Opt. Fiber Commun. Conf. Exhib.*, 2020, Paper Th3K.4, doi: 10.1364/OFC.2020.Th3K.4.

[6] L. Xue, R. Lin, J. V. Kerrebrouck, L. Yi, J. Chen, and X. Yin, "100G PAM-4 PON with 34 dB power budget using joint nonlinear tomlinson-harashima precoding and volterra equalization," in *Proc. Eur. Conf. Opt. Commun.*, 2021, pp. 1–4, doi: 10.1109/ECOC52684.2021.9606041.

[7] D. Che, P. Iannone, G. Raybon, and Y. Matsui, "200Gb/s bi-directional TDM-PON with 29-dB power budget," in *Proc. Eur. Conf. Opt. Commun.*, 2021, pp. 1–3, doi: 10.1109/ECOC52684.2021.9606049.

[8] J. Zhang, L. Yan, L. Jiang, A. Yi, and Y. Pan, "56-Gbit/s PAM-4 optical signal transmission over 100-km SMF enabled by TCNN regression model," *IEEE Photon. J*, vol. 13, no. 4, Aug. 2021, Art. no. 7200606, doi: 10.1109/JPHOT.2021.3092003.

[9] F. Hamaoka et al., "Experimental investigation of influence of SOA-induced nonlinear distortion on high-symbol-rate 168-GBaud signal for achieving ultra-broadband optical frontend," in *Proc. Opt. Fiber Commun. Conf. Exhib.*, 2022, Paper M3H.2, doi: 10.1364/OFC.2022.M3H.2.

[10] D. F. Bendimerad and Y. Frignac, "Numerical investigation of SOA nonlinear impairments for coherent transmission systems based on SOA amplification," *J. Lightw. Technol.*, vol. 35, no. 24, pp. 5286–5295, Dec. 2017, doi: 10.1109/JLT.2017.2772223.

[11] Z. V. Rizou, K. E. Zoiros, and A. Hatziefremidis, "Comparison of basic notch filters for semiconductor optical amplifier pattern effect mitigation," *Appl. Sci.*, vol. 7, no. 8, 2017, Art. no. 783, doi: 10.3390/app7080783.

[12] G. S. Yadav, J. -H. Yan, and K. -M. Feng, "Radial basis function network equalizer for 112 Gb/s PAM4 IM-DD inter-data centers transmission with gain-clamped semiconductor optical amplifier," in *Proc. Opto-Electron. Commun. Conf.*, 2020, pp. 1–3, doi: 10.1109/OECC48412.2020.9273600.

[13] D. Semrau, D. Lavery, L. Galdino, R. I. Killey, and P. Bayvel, "The impact of transceiver noise on digital nonlinearity compensation," *J. Lightw. Technol.*, vol. 36, no. 3, pp. 695–702, Feb. 2018, doi: 10.1109/JLT.2017.2777452.

[14] C. Sun, S. H. Bae, and H. Kim, "Transmission of 28-Gb/s duobinary and PAM-4 signals using DML for optical access network," *IEEE Photon. Technol. Lett.*, vol. 29, no. 1, pp. 130–133, Jan. 2017, doi: 10.1109/LPT.2016.2629623.

[15] L. Xue, L. Yi, R. Lin, L. Huang, and J. Chen, "SOA pattern effect mitigation by neural network based pre-equalizer for 50G PON," *Opt. Exp.*, vol. 29, no. 16, pp. 24714–24722, 2021, doi: 10.1364/oe.426781.

[16] A. G. Reza and J. K. Rhee, "Nonlinear equalizer based on neural networks for PAM-4 signal transmission using DML," *IEEE Photon. Technol. Lett.*, vol. 30, no. 15, pp. 1416–1419, Aug. 2018, doi: 10.1109/LPT.2018.2852327.

[17] C. Chuang et al., "Convolutional neural network based nonlinear classifier for 112-Gbps high speed optical link," in *Proc. Opt. Fiber Commun. Conf. Exhib.*, 2018, Paper W2A.43, doi: 10.1364/OFC.2018.W2A.43.

[18] X. Huang, D. Zhang, X. Hu, C. Ye, and K. Zhang, "Recurrent neural network based equalizer with embedded parallelization for 100Gbps/λ PON," in *Proc. Opt. Fiber Commun. Conf.*, 2021, Paper M3G.2, doi: 10.1364/OFC.2021.M3G.2.

[19] A. G. Reza, M. T.-. Costas, L. P. Barry, and C. Browning, "4x75-Gbit/s optically amplified WDM-PON with beyond 31-dB power budget employing PAM-4 transmission and a recurrent neural network," in *Proc. Eur. Conf. Opt. Commun.*, 2022, Paper Tu1C.2.

[20] A. Banerjee et al., "Wavelength-division-multiplexed passive optical network (WDM-PON) technologies for broadband access: A review [Invited]," *J. Opt. Netw.*, vol. 4, no. 11, pp. 737–758, 2005, doi: 10.1364/JON.4.000737.

[21] A. Sobhanan et al., "Semiconductor optical amplifiers: Recent advances and applications," *Adv. Opt. Photon.*, vol. 14, no. 3, pp. 571–651, 2022, doi: 10.1364/aop.451872.

[22] J. Zhang et al., "SOA pre-amplified 100 Gb/s/λ PAM-4 TDM-PON downstream transmission using 10 Gbps O-Band transmitters," *J. Lightw. Technol.*, vol. 38, no. 2, pp. 185–193, Jan. 2020, doi: 10.1109/JLT.2019.2944558.

[23] R. Bonk, "SOA for future PONs," in *Proc. Opt. Fiber Commun. Conf. Exhib.*, 2018, Paper Tu2B.4, doi: 10.1364/OFC.2018.Tu2B.4.

[24] L. N. Binh, *Digital Processing: Optical Transmission and Coherent Receiving Techniques*. Boca Raton, FL, USA: CRC, 2013, doi: 10.1201/b15586.

[25] D. Li et al., "Low-complexity equalization scheme for suppressing FFE-enhanced in-band noise and ISI in 100 Gbps PAM4 optical IMDD system," *Opt. Lett.*, vol. 45, no. 9, pp. 2555–2558, 2020, doi: 10.1364/OL.392344.